

Wei CHEN, Xiang LIU, Shaojie WEI, Qianqian HENG, Binfen WANG, Shilong LIU, Li GAO, Liqun MAO

# ***In situ* growth of a-few-layered MoS<sub>2</sub> on CdS nanorod for high efficient photocatalytic H<sub>2</sub> production**

© Higher Education Press 2021

**Abstract** An ultrathin MoS<sub>2</sub> was grown on CdS nanorod by a solid state method using sulfur powder as sulfur source for photocatalytic H<sub>2</sub> production. The characterization result reveals that the ultrathin MoS<sub>2</sub> nanosheets loaded on CdS has a good contact state. The photoelectrochemical result shows that MoS<sub>2</sub> not only are beneficial for charge separation, but also works as active sites, thus enhancing photocatalytic activity. Compared with pure CdS, the photocatalytic activity of MoS<sub>2</sub> loaded CdS was significantly improved. The hydrogen evolution rate on  $m(\text{MoS}_2): m(\text{CdS}) = 1: 50$  ( $m$  is mass) reaches 542  $\mu\text{mol/h}$ , which is 6 times of that on pure CdS (92  $\mu\text{mol/h}$ ). This work provides a new design for photocatalysts with high photocatalytic activities and provides a deeper understanding of the effect of MoS<sub>2</sub> on enhancing photocatalytic activity.

**Keywords** photocatalytic H<sub>2</sub> production, CdS, MoS<sub>2</sub> cocatalyst, charge separation

## **1 Introduction**

Photocatalytic H<sub>2</sub> production has been regarded as an ideal technology for clear energy [1–3]. The development of photocatalysts is the critical segment for this technology. In general, the photocatalytic activity of photocatalysts strongly depends on their absorption ability to light

photons and separation ability of photoinduced electron-hole pairs [4,5]. Therefore, the screening of photocatalysts with narrow band gaps and further modification for promoting the separation efficiency of charge are the directions of efforts for the development of photocatalysts.

CdS, a visible-light-response photocatalytic material, can absorb light not longer than 520 nm, whose energy reaches nearly half of the entire visible light [6]. Moreover, CdS possesses very suitable conduction band (CB) and valence band (VB) potentials, and meets the thermodynamic requirement for H<sub>2</sub> evolution reaction. However, the photocatalytic activity on pure CdS for H<sub>2</sub> evolution is very low due to the lack of active sites on the surface of CdS as well as the rapid recombination of photoinduced electron-hole pairs. To overcome this deficiency, some noble metals, such as Pt and Pd as cocatalysts are loaded on the surface of CdS [7]. With their high work function, noble metals facilitate the transfer of electrons from CdS to their surface while holes remain on CdS, causing the separation of electrons and holes. Apparently, although noble metals have excellent performance for promoting photocatalytic activity, they are expensive and rare, which is detrimental to the practical application on a large scale. Recently, non-noble metal sulfides, such as NiS, CoS<sub>2</sub>, and MoS<sub>2</sub> have been regarded as good substitutes for noble metal cocatalysts [8–11]. With the same type of characteristic as CdS, metal sulfide cocatalysts tend to have better interface contacts with CdS, thus facilitating the charge transfer. Among the many metal sulfide cocatalysts, the two-dimensional (2D) layered material MoS<sub>2</sub> has received more attention due to the very low free energy of H adsorption on its edge sites [12]. Moreover, MoS<sub>2</sub> with a single or few layers possesses a much better performance than bulk MoS<sub>2</sub> because of the lower charge transfer resistance [13].

As a typical layered material, MoS<sub>2</sub> stacked nanosheets are formed by the growth of three stacked atom layers (S-Mo-S). Therefore, ultrathin MoS<sub>2</sub> nanosheets can be obtained by controlling the growth in the direction of the  $z$  axis or exfoliating bulk MoS<sub>2</sub>. Currently, the liquid phase

Received Mar. 13, 2021; accepted Jul. 23, 2021; online Sept. 15, 2021

Wei CHEN (✉), Xiang LIU, Shaojie WEI, Qianqian HENG, Binfen WANG, Shilong LIU, Li GAO (✉), Liqun MAO  
Henan Engineering Research Center of Resource and Energy Recovery from Waste, Henan University, Kaifeng 475004, China  
E-mails: chanwee@henu.edu.cn (Wei CHEN);  
gaoli@henu.edu.cn (Li GAO)

Special Issue—Photocatalysis: From Solar Light to Hydrogen Energy  
(Guest Editors: Wenfeng SHANGGUAN, Akihiko KUDO, Zhi JIANG, Yuichi YAMAGUCHI)

exfoliation (LPE) method was widely used for obtaining mono- or several-layered MoS<sub>2</sub> by ultrasonating bulk MoS<sub>2</sub> to destroy the van der Waals force between two adjacent layers [14–17]. Unfortunately, the yield of the ultrathin MoS<sub>2</sub> was comparatively low and went against the particle application. Additionally, using MoO<sub>3</sub> and S powder as precursors for deposition of MoS<sub>2</sub> on substrates, the high quality ultrathin MoS<sub>2</sub> could be prepared by utilizing a chemical vapor deposition (CVD) method [18]. However, its complex preparation process also limited its application on a large scale. Therefore, the development of a simple method for preparing ultrathin MoS<sub>2</sub> to enhance activity is of great significance.

Herein, a simple method was used to load ultrathin MoS<sub>2</sub> on the surface of CdS nanorod for promoting the photocatalytic activity. The *in-situ* growth of MoS<sub>2</sub> on CdS would lead to a strong interface contact between them, which would facilitate the charge transfer and enhance the photocatalytic activity. First, nano Mo species were loaded and fastened on the CdS nanorod. Then, the S powder vulcanized Mo species to form ultrathin MoS<sub>2</sub>. The MoS<sub>2</sub> was loaded on CdS due to its strong 2D orientation. The morphology of few-layered MoS<sub>2</sub> on CdS nanorod was verified. The performance and roles of ultrathin MoS<sub>2</sub> on enhancing photocatalytic activity were investigated.

## 2 Experimental

### 2.1 Material synthesis

Cadmium nitrate, thiourea, sulfur and 1,2-ethylenediamine (en) were purchased from Macklin (Shanghai, China). Ammonium molybdate and lactic acid were purchased from Sinopharm Chemical Reagent Co. Ltd. China.

CdS nanorod was synthesized by utilizing a solvothermal method. 3.08 g of cadmium nitrate and 2.28 g of thiourea were dissolved into 48 mL of 1,2-ethylenediamine (en). After stirring for 0.5 h, the mixture was then

transferred to a sealed Teflonlined autoclave and kept at 160°C for 48 h. The obtained product was cleaned by distilled water and anhydrous alcohol. Finally, CdS nanorods, were obtained in vacuum furnace by drying at 40°C for 24 h.

The growth of MoS<sub>2</sub> on CdS nanorod was achieved by utilizing an impregnation method. 0.3 g of CdS nanorod was added into 30 mL of aqueous solution containing an appropriate amount of (NH<sub>4</sub>)<sub>6</sub>Mo<sub>7</sub>O<sub>24</sub>. Under continuous stirring, the suspension was dried by water bath at 60°C. The obtained yellow powder was mixed with 0.1 g of S powder and then vulcanized at 400°C. Finally, the powder was washed by alcohol to obtain MoS<sub>2</sub>/CdS. The mass ratios of MoS<sub>2</sub> and CdS are  $m(\text{MoS}_2):m(\text{CdS}) = 1:100$  ( $w(\text{MoS}_2) = 1\%$ ,  $w$  is mass fraction),  $m(\text{MoS}_2):m(\text{CdS}) = 1:50$  ( $w(\text{MoS}_2) = 2\%$ ) and  $m(\text{MoS}_2):m(\text{CdS}) = 1:33$  ( $w(\text{MoS}_2) = 3\%$ ), respectively. A schematic diagram of the photocatalyst synthesis is shown in Fig. 1. MoS<sub>2</sub> was also prepared by (NH<sub>4</sub>)<sub>6</sub>Mo<sub>7</sub>O<sub>24</sub> and S powder using the same method.

### 2.2 Characterization

The crystal structure of materials was confirmed by X-ray diffraction (XRD, Bruker-AXS, Cu K $\alpha$ ,  $\lambda = 0.15406$  nm). The morphology and energy dispersive X-Ray spectroscopy (EDX) analysis of samples were characterized by using high resolution transmission electron microscopy (HRTEM) at 200 kV (FEI Talos F200, USA). The UV-vis diffuse reflection spectra (DRS) were determined by a UV-vis spectrophotometer TU-1901 (Purkinje, China) and were converted to absorbance by using a Kubelka-Munk method. The surface electronic state was analyzed by using X-ray photoelectron spectroscopy (XPS, Shimadzu-Kratos, Axis UltraDLD, Japan). All the binding energy (BE) values were calibrated by using the standard BE value of contaminant carbon (C 1s = 284.6 eV) as a reference. Photoluminescence (PL) spectra were recorded using an Edinburgh FLS980 fluorescence spectrometer with an

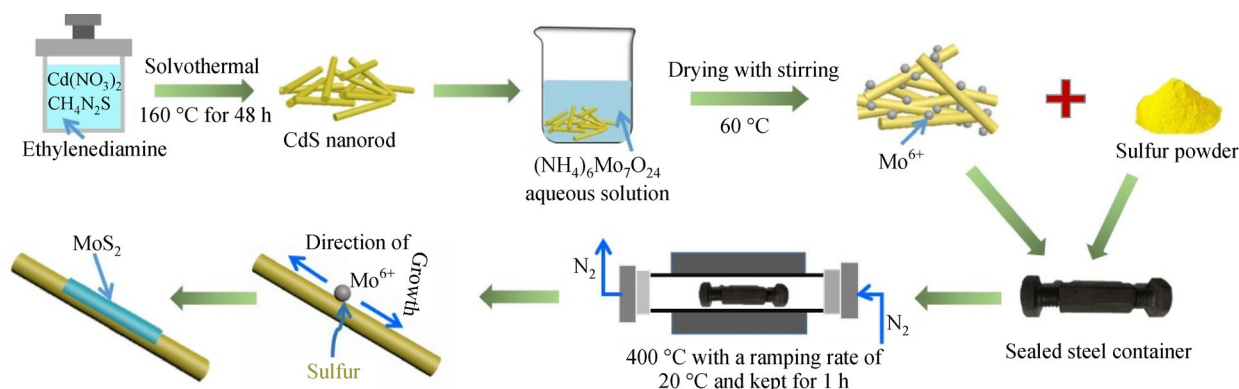


Fig. 1 Schematic illustration of the synthesis procedure to obtain MoS<sub>2</sub>/CdS nanorod.

excitation light wavelength of 325 nm. Linear sweep voltammetry (LSV), photocurrent response ( $I-t$ ), electrochemical impedance spectroscopy (EIS), and Mott-Schottky measurements were performed on a CH Instrument 760D electrochemical workstation (Chenhua, Shanghai) using a 0.5 mol/L  $\text{Na}_2\text{SO}_4$  aqueous solution as the electrolyte.

### 2.3 Photocatalytic activity for $\text{H}_2$ evolution

Photocatalytic  $\text{H}_2$  production was achieved in a 350 mL reactor, which contained 50 mg of CdS and 70 mL of lactic acid aqueous solution ( $V(\text{lactic acid}): V(\text{water}) = 1: 5$ ,  $V$  is volume). Subsequently, the reaction was connected with a vacuum system to remove the air. A 300 W Xe lamp ( $\lambda > 420$  nm) was used as light source. The generated  $\text{H}_2$  was detected by a gas chromatography with a thermal conductivity detector (TCD) detector.

## 3 Results and discussion

Figure 2 demonstrates the XRD patterns of CdS,  $\text{MoS}_2/\text{CdS}$ , and  $\text{MoS}_2$ . The main diffraction peaks of CdS at  $24.8^\circ$ ,  $26.5^\circ$ ,  $28.2^\circ$ , and  $43.7^\circ$  correspond to (100), (002), (101), and (110) plane of CdS with a hexagonal structure, respectively. For  $\text{MoS}_2$ , the diffraction peaks at  $14.4^\circ$ ,  $32.7^\circ$ , and  $39.6^\circ$  correspond to the (002), (100), and (103) planes of hexagonal  $\text{MoS}_2$  (JPCDS 65-1951), respectively, indicating that  $\text{MoS}_2$  can be prepared by S powder as S source. No diffraction peak belonging to  $\text{MoS}_2$  is observed in  $\text{MoS}_2/\text{CdS}$  samples, which should be attributed to the low loading amounts and/or the low diffraction intensity. Figure 3(a) presents the DRS spectra of pure CdS,  $\text{MoS}_2$  and  $m(\text{MoS}_2): m(\text{CdS}) = 1: 50$ . The absorption edge of CdS is approximately 520 nm, corresponding to a band gap of 2.4 eV [19]. The performance of light absorption implies that the CdS

nanorod has a hexagonal phase.  $\text{MoS}_2$  exhibits a strong absorption in the entire visible light region (400–800 nm), which should be attributed to its narrow band gap (1.1 eV) [20]. From Fig. 3(b), it can be observed that the band gap of CdS does not change after  $\text{MoS}_2$  loading, suggesting that  $\text{MoS}_2$  only supports on CdS and does not change the crystal lattice of CdS. However, after  $\text{MoS}_2$  loading,  $m(\text{MoS}_2): m(\text{CdS}) = 1: 50$  exhibits a new light absorption longer than 520 nm, which should be attributed to the adsorption of  $\text{MoS}_2$ . The adsorption peaks at approximately 620 nm and 670 nm originate from the K point of the Brillouin zone of  $\text{MoS}_2$  [21], which confirms that  $\text{MoS}_2$  has been loaded on the surface of CdS successfully.

The chemical composition and the state of the elements in  $m(\text{MoS}_2): m(\text{CdS}) = 1: 100$  were analyzed by XPS. A survey of the XPS spectrum of  $\text{MoS}_2/\text{CdS}$  (Fig. 4(a)) indicates that Cd, S, Mo, and O elements exist in  $\text{MoS}_2/\text{CdS}$ . Two peaks located at 411.8 and 405.1 eV can be observed in the XPS spectrum of Cd 3d (Fig. 4(b)), matching the binding energies of Cd  $3d_{5/2}$  and Cd  $3d_{3/2}$  and of CdS [22]. From Fig. 4(c), it can be noticed that the XPS spectrum of S 2p can be fitted to two peaks at 162.7 and 161.5 eV, corresponding to the binding energies of S  $2p_{1/2}$  and S  $2p_{3/2}$  of  $\text{S}^{2-}$  [23]. In Fig. 4(d), the Mo 3d spectrum is assigned to three peaks. The two peaks at 232.2 and 229.0 eV can be matched with the Mo  $3d_{3/2}$  and Mo  $3d_{5/2}$  of  $\text{MoS}_2$ , respectively [24]. In addition, the peak at 225.8 eV is related to the BE of S 2s of  $\text{S}^{2-}$ . Therefore, the XPS analysis confirms the successful preparation of  $\text{MoS}_2/\text{CdS}$ .

To present the microstructure of  $\text{MoS}_2$  and CdS, the  $m(\text{MoS}_2): m(\text{CdS}) = 1: 50$  sample was investigated by HRTEM. Figure 5(a) shows that CdS has a rod-like structure with a length of 200–300 nm and a width of 30–50 nm. Figures 5(b) and 5(c) shows that the  $\text{MoS}_2$  loaded on the surface of CdS nanorod possesses an ultrathin nanosheet structure. The lattice spacing of 0.62 nm and 0.23 nm corresponds to the (002) and (103) of hexagonal  $\text{MoS}_2$ , respectively, which is consistent with the XRD results [24]. A few-layered  $\text{MoS}_2$  possesses more active sites, thus promoting the photocatalytic activity [25]. In addition, Fig. 5(c) shows that a few-layered  $\text{MoS}_2$  nanosheets are in close contact with the CdS nanorods, which is greatly conducive to the charge migration between CdS and  $\text{MoS}_2$  [26]. The elemental mapping images (Fig. 5(d)) clearly reveal the ultrathin  $\text{MoS}_2$  loaded on the surface of CdS nanorod. Moreover, the EDX spectrum also indicates the existence of Mo, Cd, and S elements, suggesting that  $\text{MoS}_2$  has been loaded on the surface of CdS nanorod successfully.

The photocatalytic activity for  $\text{H}_2$  evolution on CdS and  $\text{MoS}_2/\text{CdS}$  were examined under visible light ( $\lambda > 420$  nm) when lactic acid was used as a sacrificial reagent (Fig. 6(a)). From Fig. 6(a), it can be seen that pure CdS exhibits a low photocatalytic activity for  $\text{H}_2$  evolution (92  $\mu\text{mol/h}$ ) due to the rapid charge recombination on the

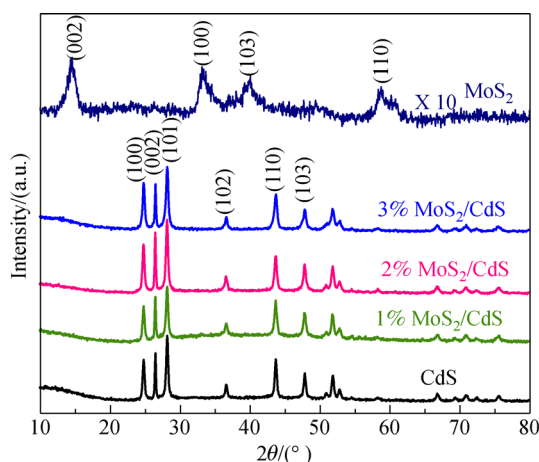
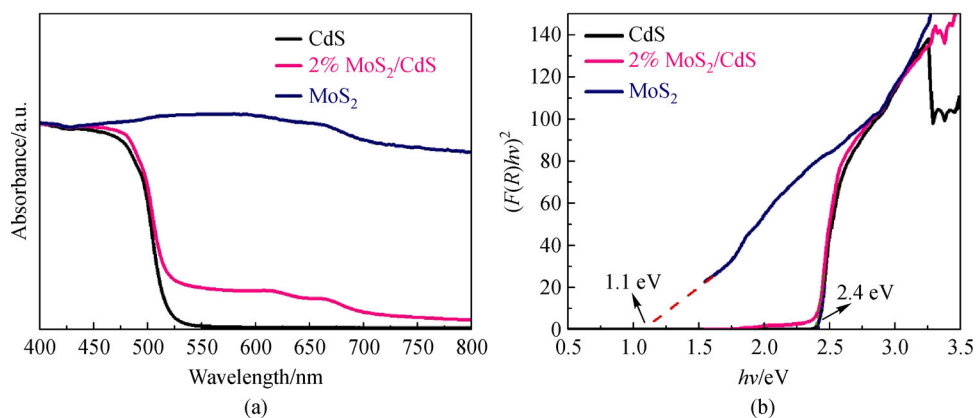
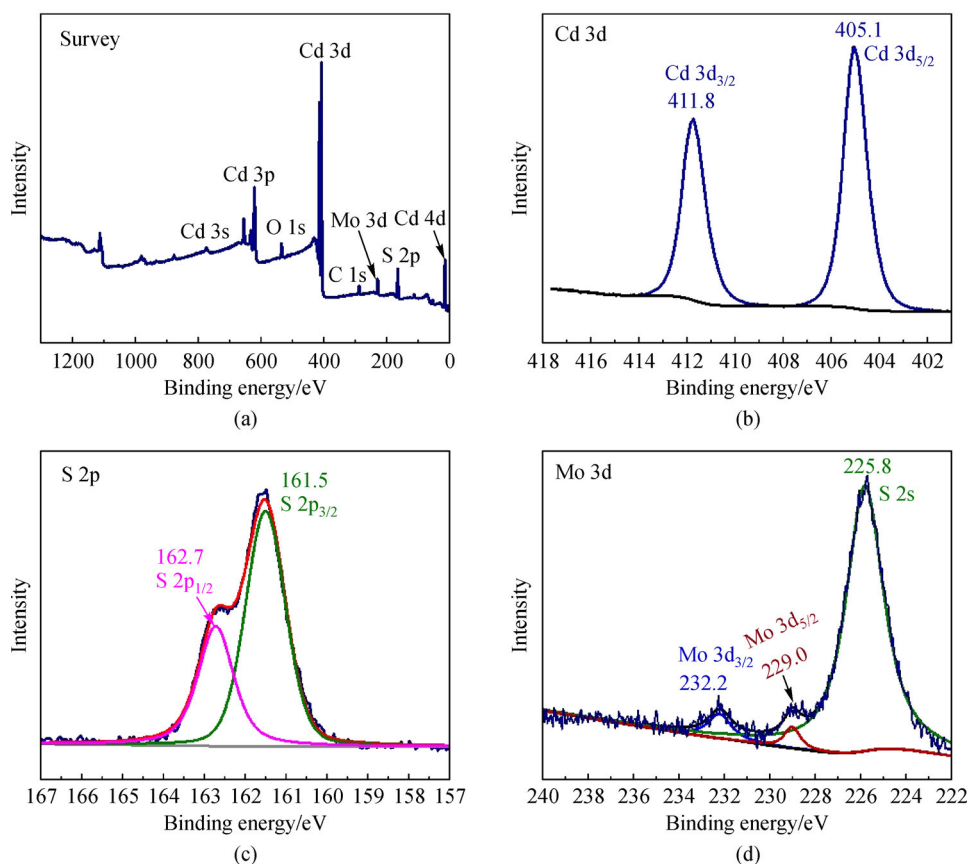


Fig. 2 XRD patterns of CdS,  $\text{MoS}_2/\text{CdS}$ , and  $\text{MoS}_2$ .



**Fig. 3** Comparison of CdS and MoS<sub>2</sub> with  $m(\text{MoS}_2): m(\text{CdS}) = 1: 50$ .  
(a) DRS spectra; (b) estimated band gaps.



**Fig. 4** XPS spectra of  $m(\text{MoS}_2): m(\text{CdS}) = 1: 100$  nanorod.  
(a) Survey; (b) Cd 3d; (c) S 2p; (d) Mo 3d and S 2s.

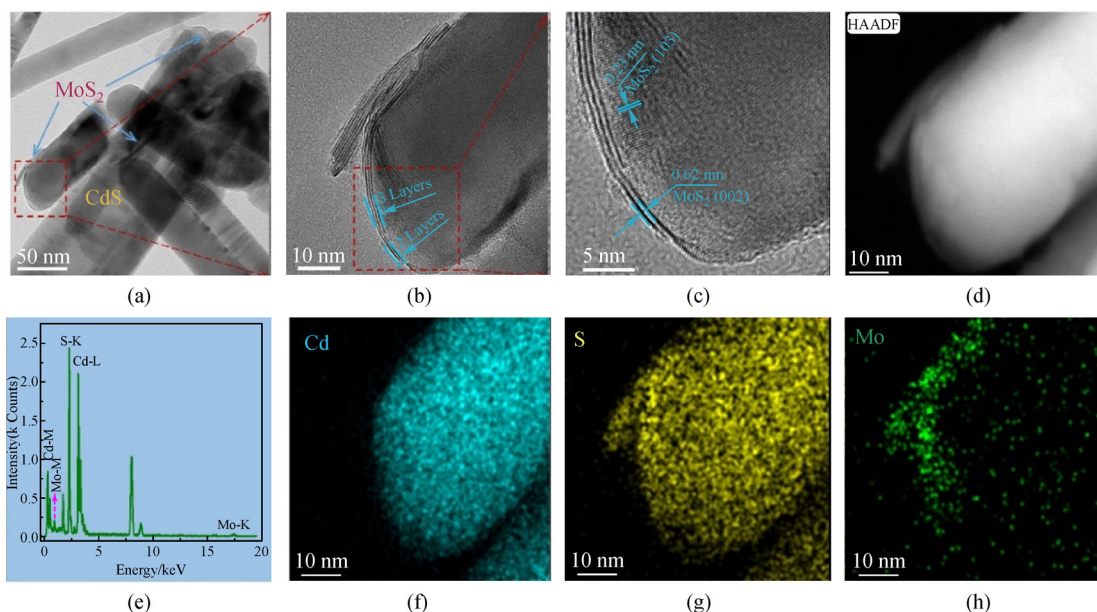
surface of CdS. Under the same experimental conditions, after MoS<sub>2</sub> loading, the photocatalytic hydrogen production rates were significantly increased. The hydrogen production rates of the MoS<sub>2</sub>/CdS catalysts loaded with  $w(\text{MoS}_2) = 1\%$ ,  $w(\text{MoS}_2) = 2\%$  and  $w(\text{MoS}_2) = 3\%$  increases first and then decreases. The photocatalytic hydrogen production rate of  $m(\text{MoS}_2): m(\text{CdS}) = 1: 50$  reaches 542  $\mu\text{mol/h}$ , which is 6 times that of pure CdS and

is also higher than that of most of the studies conducted previously, as summarized in Table 1. The result suggests that the sulfide MoS<sub>2</sub> is a good substitute for precious metals in photocatalytic hydrogen production. However, the H<sub>2</sub> evolution rate decreases when the loading amount is more than  $m(\text{MoS}_2): m(\text{CdS}) = 1: 50$ , probably as excessive MoS<sub>2</sub> on surface of CdS would become the recombination center of electrons and holes. To examine

the stability of photocatalyst, a cyclic experiment of photocatalytic reaction on  $m(\text{MoS}_2): m(\text{CdS}) = 1: 50$  was conducted. After each photocatalytic experiment was completed, the photocatalyst was washed with deionized water and dried for the next photocatalytic experiment. As manifested in Fig. 6(b), the hydrogen production performance of  $m(\text{MoS}_2): m(\text{CdS}) = 1: 50$  does not decrease during four experimental cycles, indicating the good stability of  $\text{MoS}_2/\text{CdS}$ .

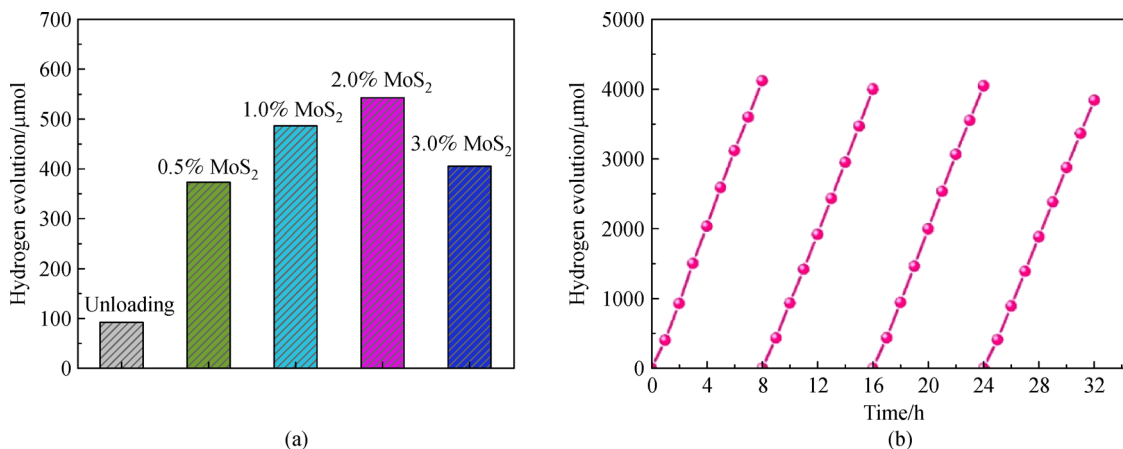
To realize a photocatalytic reaction, photocatalysts need to have not only suitable energy band potentials but also good abilities to separate photogenerated electrons and holes. Although CdS has enough negative CB potentials to reduce protons ( $\text{H}^+$ ) to  $\text{H}_2$ , the lack of active sites for  $\text{H}_2$

evolution on the surface of CdS results in a low  $\text{H}_2$  evolution efficiency. To probe the effect of  $\text{MoS}_2$  on enhancing the photocatalytic activity of CdS, a photoelectrochemical test was conducted. Figure 7(a) depicts the LSV curves of pure CdS and  $\text{MoS}_2$  loaded CdS. It can be seen that pure CdS exhibits a low reduction current density, indicating that the occurrence of  $\text{H}_2$  evolution reaction on the surface of CdS is difficult. After  $\text{MoS}_2$  loading, the reduction current density of CdS is obviously promoted, implying that the  $\text{H}_2$  evolution reaction occurs on the surface of  $\text{MoS}_2$  easily [27,28]. Similarly, compared with pure CdS,  $m(\text{MoS}_2): m(\text{CdS}) = 1: 50$  shows a smaller semicircle arc in EIS curves (Fig. 7(d)), suggesting that the charge transfer resistance between photocatalyst and water



**Fig. 5** HRTEM images of  $\text{MoS}_2$  loaded CdS.

(a) HRTEM image in 50 nm; (b) HRTEM image in 10 nm; (c) HRTEM image in 5 nm; (d) EDX mapping; (e) EDX spectrum of  $m(\text{MoS}_2): m(\text{CdS}) = 1: 50$ ; (f) Cd element; (g) S element; (h) Mo element.

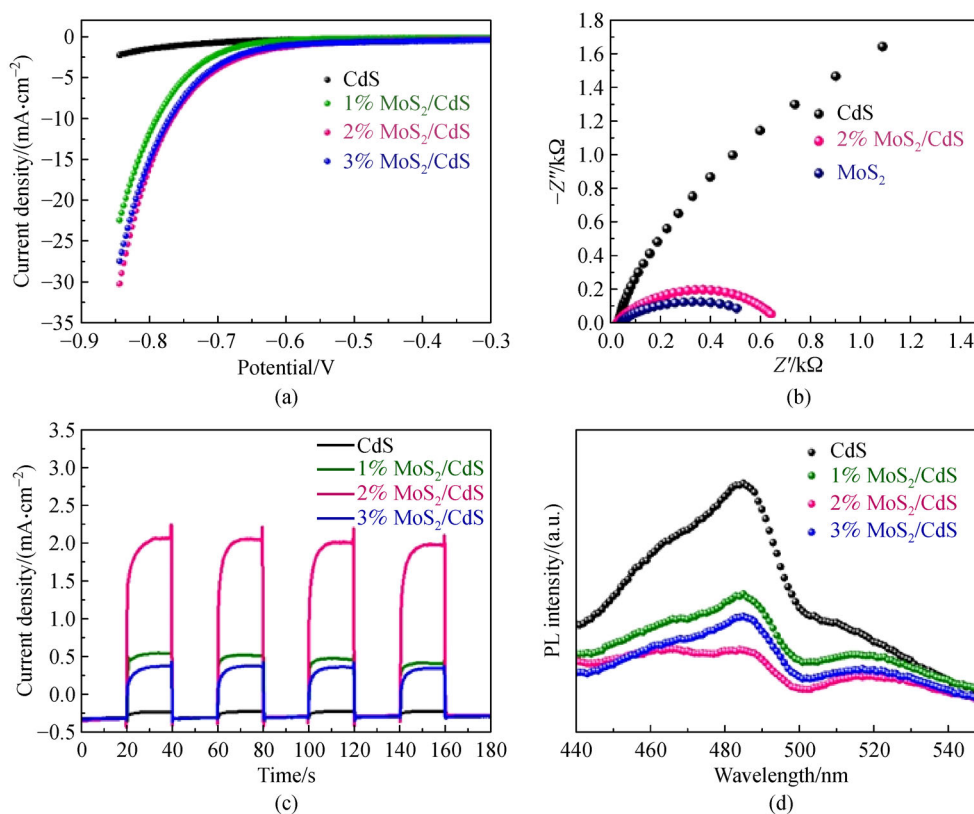


**Fig. 6** Photocatalytic  $\text{H}_2$  evolution rates of  $\text{MoS}_2$  loaded CdS.

(a) Photocatalytic activity for  $\text{H}_2$  evolution on  $\text{MoS}_2/\text{CdS}$  with different loading amounts; (b) time course of photocatalytic  $\text{H}_2$  evolution on  $m(\text{MoS}_2): m(\text{CdS}) = 1: 50$ .

**Table 1** Comparison of H<sub>2</sub> evolution rates of the current work and previous studies

Photo-catalyst	Catalyst dosage /mg	Cocatalyst / (mass fraction, %)	Preparation method	Sacrificial reagent	Light source	H <sub>2</sub> evolution rate / (μmol · h <sup>-1</sup> · g <sup>-1</sup> )	Ref.
CdS	50	2.0% MoS <sub>2</sub>	Solid state (S powder)	Lactic acid	300 W Xenon lamp, λ > 420 nm	10840	This work
CdS	50	5% MoS <sub>2</sub>	Hydrothermal	Amoxicillin	300 W Xenon lamp, λ > 420 nm	1760	[10]
CdS	100	3% MoS <sub>2</sub>	Solid state (H <sub>2</sub> S)	Lactic acid	300 W Xenon lamp, λ > 420 nm	5330	[11]
CdS	300	1.0% NiS	Hydrothermal	Lactic acid	300 W Xenon lamp, λ > 420 nm	7000	[8]
CdS	200	2% MoS <sub>2</sub>	Adsorption	Lactic acid	300 W Xenon lamp, λ > 420 nm	12950	[14]
CdS	20	25% MoS <sub>2</sub>	Hydrothermal	TEOA	300 W Xenon lamp, λ > 400 nm	1145	[19]
CdS	10	6.39% MoS <sub>2</sub>	Hydrothermal	Na <sub>2</sub> S + Na <sub>2</sub> SO <sub>3</sub>	300 W Xenon lamp, λ > 420 nm	4540	[22]

**Fig. 7** Photoelectrochemical performance of MoS<sub>2</sub>/CdS. (a) LSV curves; (b) EIS plots; (c) amperometric *I-t* curves; (d) PL spectra of MoS<sub>2</sub>/CdS.

is reduced [29,30]. These results indicate that the H<sub>2</sub> evolution reduction reaction is more likely to occur.

To examine the charge separation ability of MoS<sub>2</sub>, the transient photocurrent and PL measurements of CdS and MoS<sub>2</sub> loaded CdS were performed. As exhibited in Fig. 7(c), pure CdS exhibits a very low photocurrent density, indicating the strong recombination of carriers on

its surface. After MoS<sub>2</sub> loading, the photocurrent density is significantly enhanced, indicating that MoS<sub>2</sub> can promote the charge separation of carriers [31,32]. The *m*(MoS<sub>2</sub>):*m*(CdS) = 1: 50 has the highest photocurrent density, revealing the best charge separation efficiency. However, the photocurrent density becomes low when the loading amount exceeds *w*(MoS<sub>2</sub>) = 2%, suggesting that excessive

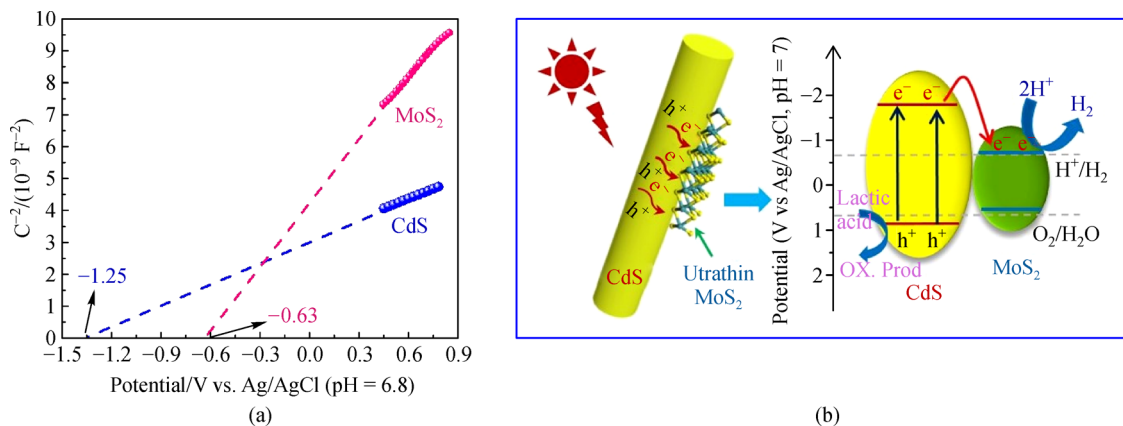


**Fig. 8** Mechanism of charge separation of MoS<sub>2</sub>/CdS.

(a) Mott-Schottky spots of CdS and MoS<sub>2</sub>; (b) schematic of enhanced charge separation and photocatalytic activity of MoS<sub>2</sub>/CdS.

MoS<sub>2</sub> results in a low photoelectric conversion efficiency. A similar tendency also appears in the PL measured result (Fig. 7(d)), which represents the level of recombination of carriers [33,34]. Clearly, pure CdS possesses the strongest PL intensity. After MoS<sub>2</sub> loading, the PL intensity decreases, implying the charge separation efficiency is enhanced. However, the PL intensity of  $m(\text{MoS}_2):m(\text{CdS}) = 1:33$  becomes stronger than that of  $m(\text{MoS}_2):m(\text{CdS}) = 1:50$ , indicating that excessive MoS<sub>2</sub> would become the center of recombination, thus reducing the photocatalytic activity [35,36].

Based on the analysis mentioned above, the mechanism of loaded MoS<sub>2</sub> in enhancing the photocatalytic activity for H<sub>2</sub> evolution can be explained as follows: Under visible light irradiation, the electrons are generated from the VB of CdS to its CB. However, for pure CdS, because of the lack of active sites, the electrons rapidly recombine with holes. After MoS<sub>2</sub> loading, because the CB potential of MoS<sub>2</sub> (−0.63 V versus Ag/AgCl, pH = 6.8) is lower than that of CdS (−1.25 V versus Ag/AgCl, pH = 6.8), the electrons from the CB of CdS are likely to transfer to the CB of MoS<sub>2</sub>, resulting in the separation of electrons and holes in space (Fig. 8). The ultrathin structure of MoS<sub>2</sub> loaded on CdS shortens the migration distance of electron from CdS to MoS<sub>2</sub>, facilitating charge separation. Moreover, the reduction reaction of protons is more likely to happen on the surface of MoS<sub>2</sub>, further enhancing the photocatalytic activity. However, excessive MoS<sub>2</sub> will cover the surface of CdS, which blocks the light absorption and becomes the recombination center of electron and holes, thus decreasing the photocatalytic activity.

## 4 Conclusions

In summary, a few-layered MoS<sub>2</sub> was loaded on CdS nanorod by utilizing a solid state method using sulfur powder as sulfur source for photocatalytic H<sub>2</sub> production.

Based on the difference of CB potential in CdS and MoS<sub>2</sub>, the electrons from CdS tend to transfer to MoS<sub>2</sub>, which results in a high charge separation efficiency. The ultrathin structure of MoS<sub>2</sub> on CdS shortens the migration distance of electron from CdS to MoS<sub>2</sub>, facilitating charge separation. Moreover, the reduction reaction of proton is more likely to occur on the surface of MoS<sub>2</sub> further enhancing photocatalytic activity. Compared with CdS, the photocatalytic activity of MoS<sub>2</sub> loaded CdS is significantly improved. The hydrogen evolution rate of  $m(\text{MoS}_2):m(\text{CdS}) = 1:50$  reaches 542 μmol/h, which is 6 times of that on pure CdS (92 μmol/h). This work gives a new design for photocatalysts with high photocatalytic activity and provides a deeper understanding of cocatalysts on enhancing photocatalytic activity.

**Acknowledgements** This work was supported by the National Natural Science Foundation of China (Grant No. 51602091) and the Project of Department of Science and Technology of Henan Province (182102210228).

## References

1. Takata T, Jiang J, Sakata Y, et al. Photocatalytic water splitting with a quantum efficiency of almost unity. *Nature*, 2020, 581(7809): 411–414
2. Kranz C, Wächtler M. Characterizing photocatalysts for water splitting: from atoms to bulk and from slow to ultrafast processes. *Chemical Society Reviews*, 2021, 50(2): 1407–1437
3. Fang X, Kalathil S, Reisner E. Semi-biological approaches to solar-to-chemical conversion. *Chemical Society Reviews*, 2020, 49(14): 4926–4952
4. Ran J, Zhang J, Yu J, et al. Earth-abundant cocatalysts for semiconductor-based photocatalytic water splitting. *Chemical Society Reviews*, 2014, 43(22): 7787–7812
5. Lin L, Yu Z, Wang X. Crystalline carbon nitride semiconductors for photocatalytic water splitting. *Angewandte Chemie International Edition*, 2019, 58(19): 6164–6175

- Chen W, Wang Y, Liu M, et al. In situ photodeposition of cobalt on CdS nanorod for promoting photocatalytic hydrogen production under visible light irradiation. *Applied Surface Science*, 2018, 444: 485–490
- Yan H, Yang J, Ma G, et al. Visible-light-driven hydrogen production with extremely high quantum efficiency on Pt-PdS/CdS photocatalyst. *Journal of Catalysis*, 2009, 266(2): 165–168
- Zhang W, Wang Y, Wang Z, et al. Highly efficient and noble metal-free NiS/CdS photocatalysts for H<sub>2</sub> evolution from lactic acid sacrificial solution under visible light. *Chemical Communications: Cambridge, England*, 2010, 46(40): 7631–7633
- Qiu B, Li C, Shen X, et al. Revealing the size effect of metallic CoS<sub>2</sub> on CdS nanorods for photocatalytic hydrogen evolution based on Schottky junction. *Applied Catalysis A, General*, 2020, 592: 117377
- Xu M, Wei Z, Liu J, et al. One-pot synthesized visible-light-responsive MoS<sub>2</sub>@CdS nanosheets-on- nanospheres for hydrogen evolution from the antibiotic wastewater: waste to energy insight. *International Journal of Hydrogen Energy*, 2019, 44(39): 21577–21587
- Zong X, Wu G, Yan H, et al. Photocatalytic H<sub>2</sub> evolution on MoS<sub>2</sub>/CdS catalysts under visible light irradiation. *Journal of Physical Chemistry C*, 2010, 114(4): 1963–1968
- Zhang G, Liu H, Qu J, et al. Two-dimensional layered MoS<sub>2</sub>: rational design, properties and electrochemical applications. *Energy & Environmental Science*, 2016, 9(4): 1190–1209
- Jaramillo T F, Jørgensen K P, Bonde J, et al. Identification of active edge sites for electrochemical H<sub>2</sub> evolution from MoS<sub>2</sub> nanocatalysts. *Science*, 2007, 317(5834): 100–102
- Zhai Z, Yan W, Dong L, et al. Multi-dimensional materials with layered structures for supercapacitors: advanced synthesis, supercapacitor performance and functional mechanism. *Nano Energy*, 2020, 78: 105193
- Chang L, Sun Z, Hu Y. 1T phase transition metal dichalcogenides for hydrogen evolution reaction. *Electrochemical Energy Reviews*, 2021, 4(2): 194–218
- Liu X, Wang B, Liu M, et al. *In situ* growth of vertically aligned ultrathin MoS<sub>2</sub> on porous g-C<sub>3</sub>N<sub>4</sub> for efficient photocatalytic hydrogen production. *Applied Surface Science*, 2021, 554: 149617
- Chang K, Li M, Wang T, et al. Drastic layer-number-dependent activity enhancement in photocatalytic H<sub>2</sub> evolution over *n*MoS<sub>2</sub>/CdS (*n* ≥ 1) under visible light. *Advanced Energy Materials*, 2015, 5(10): 1402279
- Taniguchi T, Nurdiwijayanto L, Li S, et al. On/off boundary of photocatalytic activity between single- and bi-layer MoS<sub>2</sub>. *ACS Nano*, 2020, 14(6): 6663–6672
- Liu Y, Zeng C, Ai L, et al. Boosting charge transfer and hydrogen evolution performance of CdS nanocrystals hybridized with MoS<sub>2</sub> nanosheets under visible light irradiation. *Applied Surface Science*, 2019, 484: 692–700
- Yin X, Ye Z, Chenet D A, et al. Edge nonlinear optics on a MoS<sub>2</sub> atomic monolayer. *Science*, 2014, 344(6183): 488–490
- Hai X, Zhou W, Chang K, et al. Engineering the crystallinity of MoS<sub>2</sub> monolayers for highly efficient solar hydrogen production. *Journal of Materials Chemistry A, Materials for Energy and Sustainability*, 2017, 5(18): 8591–8598
- Zhao L, Jia J, Yang Z, et al. One-step synthesis of CdS nanoparticles/MoS<sub>2</sub> nanosheets heterostructure on porous molybdenum sheet for enhanced photocatalytic H<sub>2</sub> evolution. *Applied Catalysis B: Environmental*, 2017, 210: 290–296
- Wei Z, Xu M, Liu J, et al. Simultaneous visible-light-induced hydrogen production enhancement and antibiotic wastewater degradation using MoS<sub>2</sub>@Zn<sub>x</sub>Cd<sub>1-x</sub>S: solid-solution-assisted photocatalysis. *Chinese Journal of Catalysis*, 2020, 41(1): 103–113
- Chen W, Liu M, Wei S, et al. Solid-state synthesis of ultrathin MoS<sub>2</sub> as a cocatalyst on mesoporous g-C<sub>3</sub>N<sub>4</sub> for excellent enhancement of visible light photoactivity. *Journal of Alloys and Compounds*, 2020, 836: 155401
- Xu J, Zhang J, Zhang W, et al. Interlayer nanoarchitectonics of two-dimensional transition-metal dichalcogenides nanosheets for energy storage and conversion applications. *Advanced Energy Materials*, 2017, 7(23): 1700571
- Shi X, Fujitsuka M, Kim S, et al. Faster electron injection and more active sites for efficient photocatalytic H<sub>2</sub> evolution in g-C<sub>3</sub>N<sub>4</sub>/MoS<sub>2</sub> hybrid. *Small*, 2018, 14(11): 1703277
- Chen W, Wang Y, Liu S, et al. Non-noble metal Cu as a cocatalyst on TiO<sub>2</sub> nanorod for highly efficient photocatalytic hydrogen production. *Applied Surface Science*, 2018, 445: 527–534
- Ko D, Jin X, Seong K D, et al. Few-layered MoS<sub>2</sub> vertically aligned on 3D interconnected porous carbon nanosheets for hydrogen evolution. *Applied Catalysis B: Environmental*, 2019, 248: 357–365
- Reddy D A, Kim E H, Gopannagari M, et al. Few layered black phosphorus/MoS<sub>2</sub> nanohybrid: a promising co-catalyst for solar driven hydrogen evolution. *Applied Catalysis B: Environmental*, 2019, 241: 491–498
- Liu J, Fang W, Wei Z, et al. Efficient photocatalytic hydrogen evolution on N-deficient g-C<sub>3</sub>N<sub>4</sub> achieved by a molten salt post-treatment approach. *Applied Catalysis B: Environmental*, 2018, 238: 465–470
- Liu H, Li Y, Xiang M, et al. Single-layered MoS<sub>2</sub> directly grown on rutile TiO<sub>2</sub>(110) for enhanced interfacial charge transfer. *ACS Nano*, 2019, 13(5): 6083–6089
- Ge L, Han C, Xiao X, et al. Synthesis and characterization of composite visible light active photocatalysts MoS<sub>2</sub>-g-C<sub>3</sub>N<sub>4</sub> with enhanced hydrogen evolution activity. *International Journal of Hydrogen Energy*, 2013, 38(17): 6960–6969
- Chen W, Wang Y, Shanguan W. Metal (oxide) modified (M = Pd, Ag, Au and Cu) H<sub>2</sub>SrTa<sub>2</sub>O<sub>7</sub> for photocatalytic CO<sub>2</sub> reduction with H<sub>2</sub>O: the effect of cocatalysts on promoting activity toward CO and H<sub>2</sub> evolution. *International Journal of Hydrogen Energy*, 2019, 44(8): 4123–4132
- Wei S, Heng Q, Wu Y, et al. Improved photocatalytic CO<sub>2</sub> conversion efficiency on Ag loaded porous Ta<sub>2</sub>O<sub>5</sub>. *Applied Surface Science*, 2021, 563: 150273
- Chang K, Mei Z, Wang T, et al. MoS<sub>2</sub>/graphene cocatalyst for efficient photocatalytic H<sub>2</sub> evolution under visible light irradiation. *ACS Nano*, 2014, 8(7): 7078–7087
- Chen W, Chu M, Gao L, et al. Ni(OH)<sub>2</sub> loaded on TaON for enhancing photocatalytic water splitting activity under visible light irradiation. *Applied Surface Science*, 2015, 324: 432–437